Ashish Pathak and A. K. Singh*

Transition Metal Nitrides: A First Principles Study

DOI 10.1515/htmp-2014-0169
Received September 24, 2014; accepted March 26, 2015

Abstract: The present work describes the structural stability and electronic and mechanical properties of transition metal nitrides (TmNs: B1 cubic structure (cF8, Fm $\bar{3}$ m)) using first principles density functional theory (DFT) within generalized gradient approximation (GGA). The lattice constant of TmNs increases with increasing the atomic radii of the transition metals. Stability of the TmNs decreases from IVB to VIB groups due to increase in formation energy/atom. The bonding characteristics of these nitrides have been explained based on electronic density of states and charge density. All the TmNs satisfy Born stability criteria in terms of elastic constants except CrN and MoN that do not exist in equilibrium binary phase diagrams. The groups IVB and V–VIB nitrides are associated with brittle and ductile behaviour based on G/B ratios, respectively. The estimated melting temperatures of these nitrides exhibit reasonably good agreement with calculated with B than those of the C_{11} for all nitrides.

Keywords: density functional theory, ab initio calculations, formation energy, electronic charge density and density of states, physical properties, mechanical properties

Introduction

Binary transition metal nitrides (TmNs) have been the subject of intense scientific interest and technological importance due to an attractive blend of physical and chemical properties. These properties are high melting point, ultra hardness (comparable to diamond), strength and durability, good optical, electrical and thermal conductivity and slow resistance to corrosion [1, 2]. As a result, these nitrides are widely used as refractory materials, wear and corrosion resistance, surface coating and thin film interconnections in integrated circuits. In addition, these are also used in electrochemical systems, including fuel cells, electric storage and secondary battery with low cost and high efficiency and electrocatalyst in the mass production and synthesis fields.

The structure of the TmNs is face centred cubic (fcc) with Fm $\bar{3}$ m space group (Figure 1) [3]. This is similar to that of the NaCl (cF8) prototype [3]. Crystallographic structural details of the TmN phases such as lattice, number of atoms per unit cell, space group, Pearson symbol, Wyckoff positions of atoms and their respective site symmetries are given in Table 1. It is known that the TmNs are an ordered phase and the 4(a) and 4(b) Wyckoff positions (Table 1) are occupied by Tm and N atoms, respectively.

A first principles total energy calculation of nitrides of IVB group (Ti, Zr and Hf), Nb and Mo has been carried out and corresponding structural and electronic properties have been reported [4–8]. However, a comprehensive first principles study of all the TmNs (IV–VIB groups) have been rather lacking in the literature. The present work is thus concerned with a detailed and systematic approach to investigate structural, electronic, single crystal elastic and polycrystalline bulk mechanical properties of TmNs using first principles total energy calculations. An attempt has been made to compare the results obtained in the present calculation with available experimental data.

Methodology

The present calculations have been carried out using first principles norm conserving pseudopotential method in the framework of the density functional theory (DFT) [9, 10]. The ABINIT software has been utilized for the same [11–14]. Exchange correlation effects have been treated within generalized gradient approximation (GGA) using Perdew–Burke–Ernzerhof formulation [15]. Convergence with respect to the plane wave cut-off energy has been verified and accordingly plane wave cut-off energy of 80 Ry has been used in the present calculation for TmNs. Fast Fourier transform algorithm [16] has been utilized to convert the wavefunctions between the real and reciprocal lattices. Consequently, conjugate gradient algorithm [17, 18] has been used to determine wave functions within the framework of self-consistency. The integration over the Brillouin zone (BZ)

***Corresponding author: A. K. Singh,** Defence Metallurgical Research Laboratory, Hyderabad 500058, India, E-mail: singh_ashok3@rediffmail.com
Ashish Pathak, Defence Metallurgical Research Laboratory, Hyderabad 500058, India

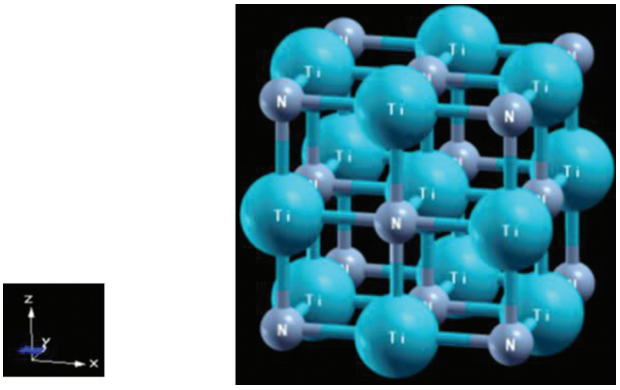

Figure 1: Crystal structure of TiN phase (B1).

Table 1: Crystallographic data of the cubic TmN phase.

TmN phase: Cubic **Fm $\bar{3}$ m; 8 atoms per unit cell** **cF8** **Atomic positions:**					
Atoms	**Wyckoff notation**	**Symmetry**	***x***	***y***	**z**
Tm	4(a)	m $\bar{3}$ m	0	0	0
N	4(b)	m $\bar{3}$ m	1/2	1/2	1/2

Note: The sum of the addition of probability of the M atoms (P_{Tm}) and probability of N atoms (P_N) on 4(a) and 4(b) sites, respectively, is 1.

has been done with the Monkhorst–Pack scheme [19]. The convergence with respect to *k*-points has been checked for different TmNs and the optimum value used for the present calculations is $6 \times 6 \times 6$ (Figure 2(a)). The periodic boundary conditions (PBCs) have been considered along ⟨100⟩ directions in real space. The structural optimization of the TmNs has been performed by relaxing the lattice constant for obtaining the minimum energy. Convergence is assumed when the differences between energies and forces in two consecutive steps are less than 27×10^{-9} meV and 2.6 meV/Å, respectively.

Both the formation energy per atom and the lattice constant **a** of TmNs at 0 K have been computed and given in Table 2. The structures of the TmNs have been initially optimized by varying the lattice constant values and corresponding equilibrium lattice constants are obtained with minimum energy. A plot of the normalized energy ratios (system energy/minimum system energy) for different TmNs along with lattice constant is shown in Figure 2(b).

The energy of formation/atom has been defined as

$$E_{for} = \frac{1}{(m+n)}(E_{Tm-N} - mE^{g}_{Tm} - nE^{g}_{N}) \quad (1)$$

where E_{Tm-N} is the total system energy of TmNs, Tm-N having m transition atoms (Tm) and n nitrogen atoms (N), E^{g}_{Tm} and E^{g}_{N} are the total energy per atom in their ground states, $(m+n)$ denotes the total number of atoms considered in the unit cell.

The elastic constants have been calculated using the linear response method implemented in ABINIT software. The linear response method is used to calculate the second derivative of the total energy with respect to the strain. The Xcrysden [20] software has been utilized for visualization of the crystal structure and 2D charge density.

Results and discussion

A first principles total energy calculation has been carried out for TmNs. A normalized energy ratio versus lattice constant plot for different TmNs is shown in Figure 2(b) and equivalent equilibrium lattice constant values are given in Table 2. The calculated lattice constant values are in good agreement with the available experimental and theoretical values [3, 5]. The calculated lattice parameter values of different TmNs depend on the size of respective transition metal [21]. For example, ZrN exhibits highest value of lattice constant because of high Seitz radius as well as high atomic volume among all transition metals (Table 2).

The calculated values of formation energy/atom of these nitrides are given in Table 2. These values do not reveal definite trend within the group; however, the values of formation energy/atom of group increase from IVB to VIB nitrides. This indicates that the stability of these nitrides decreases from IVB to VIB groups.

The electronic density of states (DOS) and 2D charge density of all the TmNs are shown in Figures 3–10. The DOS of individual atoms are also given for the comparison. Fermi level (E_F) is set at 0 eV in all the DOS figures. The highest peak observed in DOS of the TiN is located near 2.5 eV (above E_F). The locations of the highest peak appear below E_F with increase in period from TiN to HfN (Figures 3–5). The presence of these peaks is due to the contribution of individual atoms, i.e., Tm and N since they also exhibit peaks at similar positions. Therefore, the major contributions towards bonding behaviour of IVB group nitrides are due to

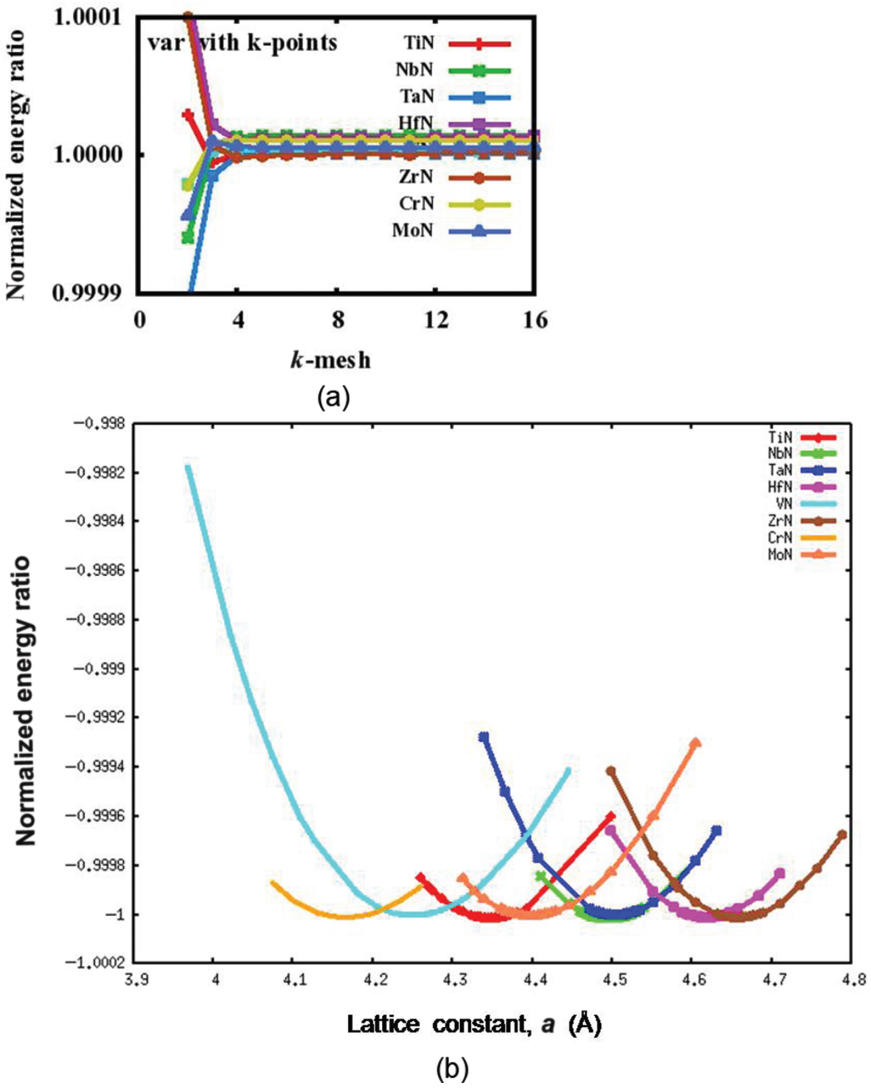

Figure 2: Variation of (a) *k*-mesh and (b) lattice parameter with normalized energy ratios for TmN.

Table 2: Equilibrium lattice constants and formation energy/atom of metal nitrides TmN (Tm = Ti, Zr, Hf, V, Nb, Ta, Cr, Mo) and corresponding atomic size and volume of Tm metals.

System	Lattice constant (Å)		Atomic size of Tm atoms		E_{for}/atom (eV)
	Present study	Expt.	Seitz radius (Å)	Atomic volume (Å^3)	
TiN	4.35	4.238	1.614	17.65	−3.024296007
ZrN	4.66	4.577	1.771	23.27	−3.105911247
HfN	4.62	4.520	1.743	22.16	−3.025780776
VN	4.25	4.137	1.491	13.88	−2.253613957
NbN	4.50	4.389	1.625	17.98	−2.262022735
TaN	4.50	4.331	1.626	18.01	−2.122243185
CrN	4.16	4.148	1.423	12.00	−1.650151855
MoN	4.40	–	1.550	15.58	−1.466222009

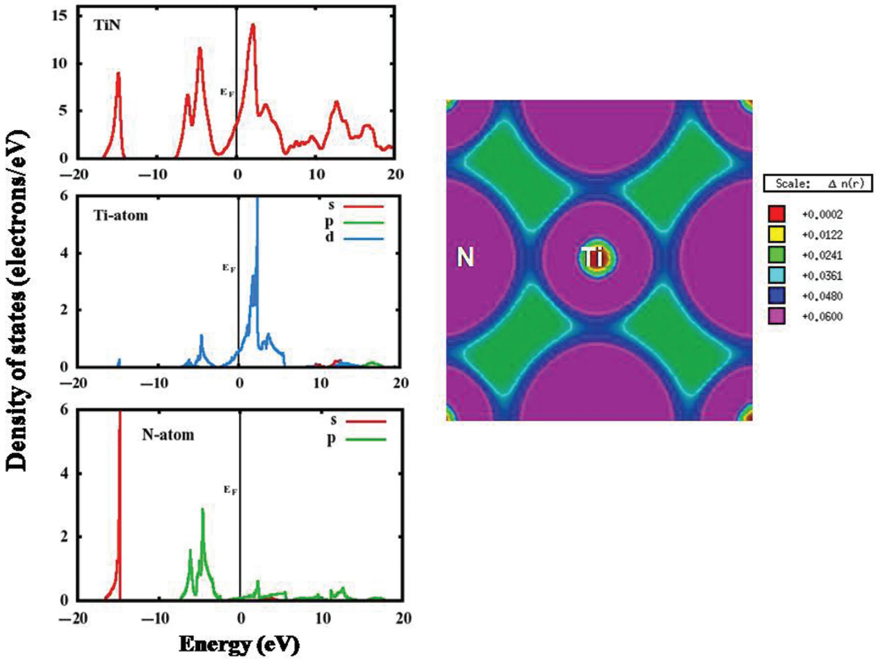

Figure 3: Electronic DOS and 2D charge density of TiN.

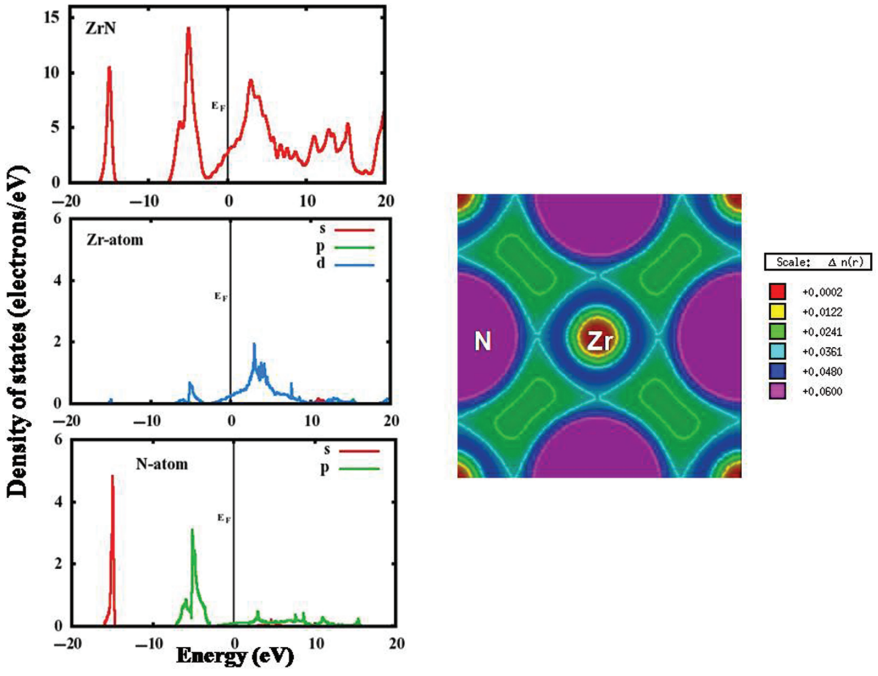

Figure 4: Electronic DOS and 2D charge density of ZrN.

Tm(d)–N(p) orbitals below E_F (Figures 3–5). Similar bonding characteristics are also observed in corresponding 2D charge density maps. The electronic charges are localized towards nitrogen atoms which is more predominant in ZrN. This can probably be attributed to a combined effect of atomic size and change in electronic structure.

The groups VB and VIB nitrides exhibit similar change in locations of the highest intensity peaks in total DOS (Figures 6–10). The bonding behaviour of these nitrides is also due to peaks below E_F exhibiting Tm (d)–N(p) orbitals. The 2D charge density maps show electronic charge localization towards N atoms and this tendency increases with increase in period in both the groups.

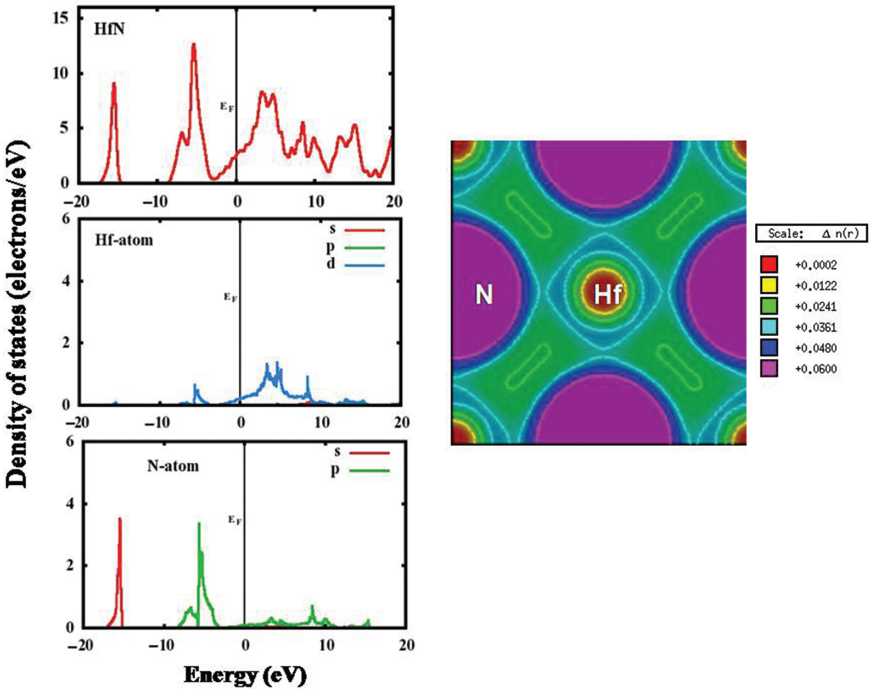

Figure 5: Electronic DOS and 2D charge density of HfN.

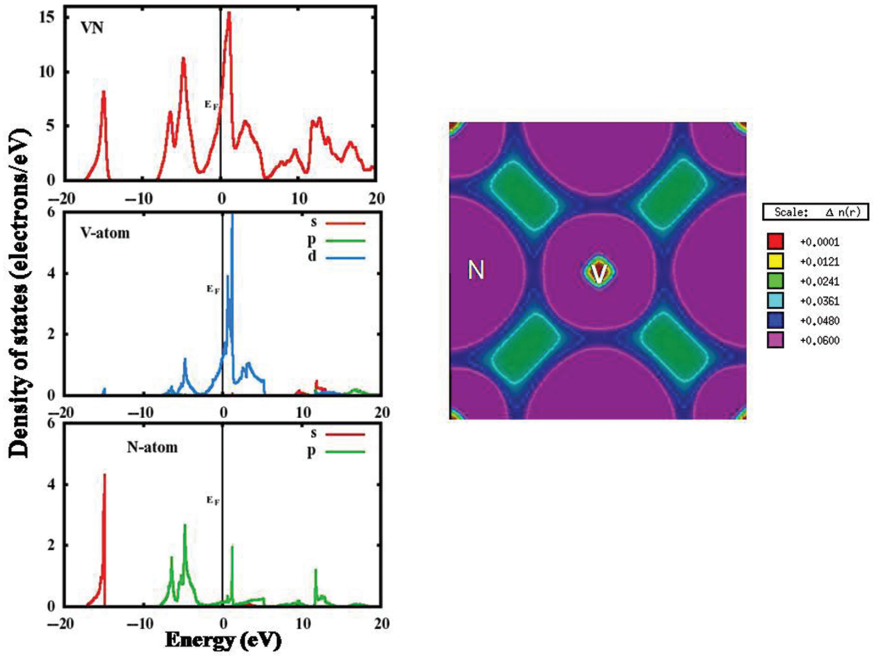

Figure 6: Electronic DOS and 2D charge density of VN.

The elastic properties of single crystal describe the behaviour of a solid that undergoes deformation and then recovers and returns to its original unstrained form. For cubic structures, the elastic properties of a single crystal are described by three elastic constants namely, C_{11}, C_{12} and C_{44}. The values of single-crystal elastic constants and available experimental data [22–25] are given in Table 3. The calculated values of elastic constants are in good agreement with experimental data available in the literature except the C_{44} values for NbN and HfN [22–25]. The elastic constant C_{11}

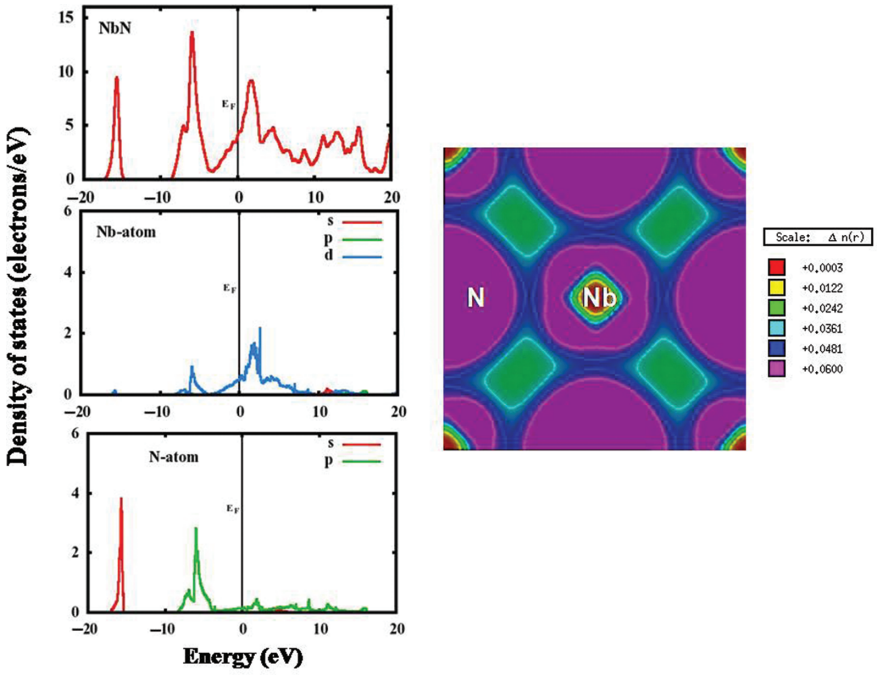

Figure 7: Electronic DOS and 2D charge density of NbN.

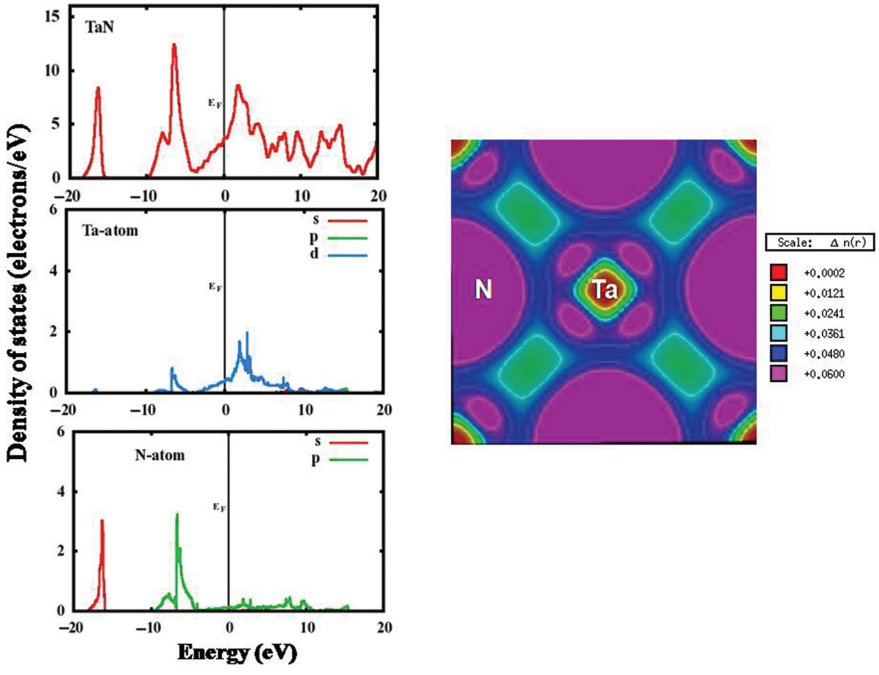

Figure 8: Electronic DOS and 2D charge density of TaN.

is significantly stiffer than those of C_{12} and C_{44}. The C_{44} values are considerably low and negative for CrN and MoN, respectively. This can be attributed to weak Tm (d)–N(p) bonding in CrN and MoN [26]. These values do not reflect systematic change within the group. This can probably be ascribed to a combined effect of atomic size of Tm atoms and corresponding electronic structure.

The nature of metallic bonding of TmNs can be predicted based on Cauchy pressure which is defined as $C_{12}-C_{44} < 0$. The negative Cauchy pressure indicates more directional bonding whereas positive value exhibits predominant metallic bonding [27, 28]. As a result, both TiN and ZrN show directional bonding while the other nitrides reflect metallic bonding [29]. The value of

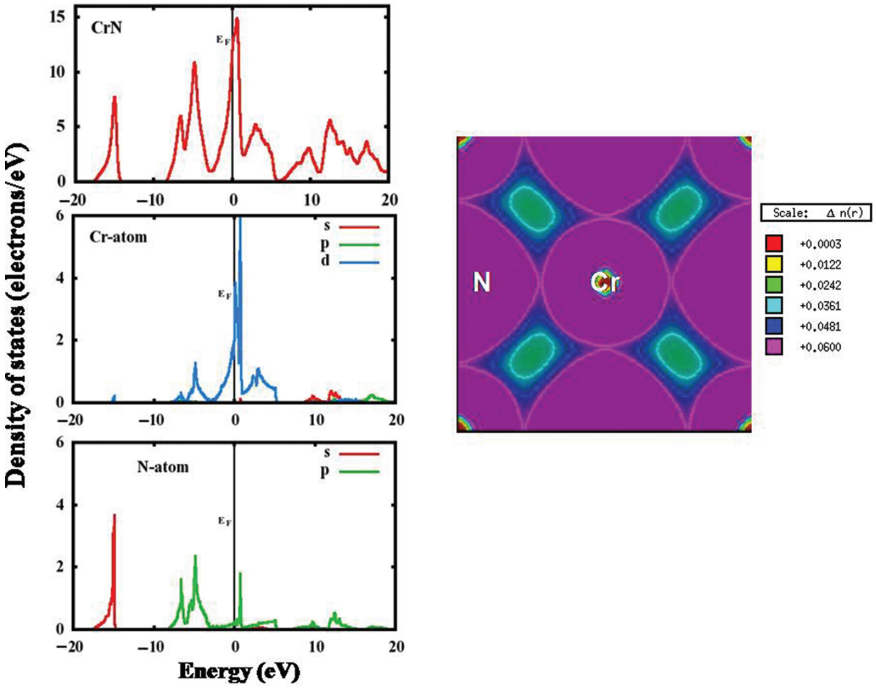

Figure 9: Electronic DOS and 2D charge density of CrN.

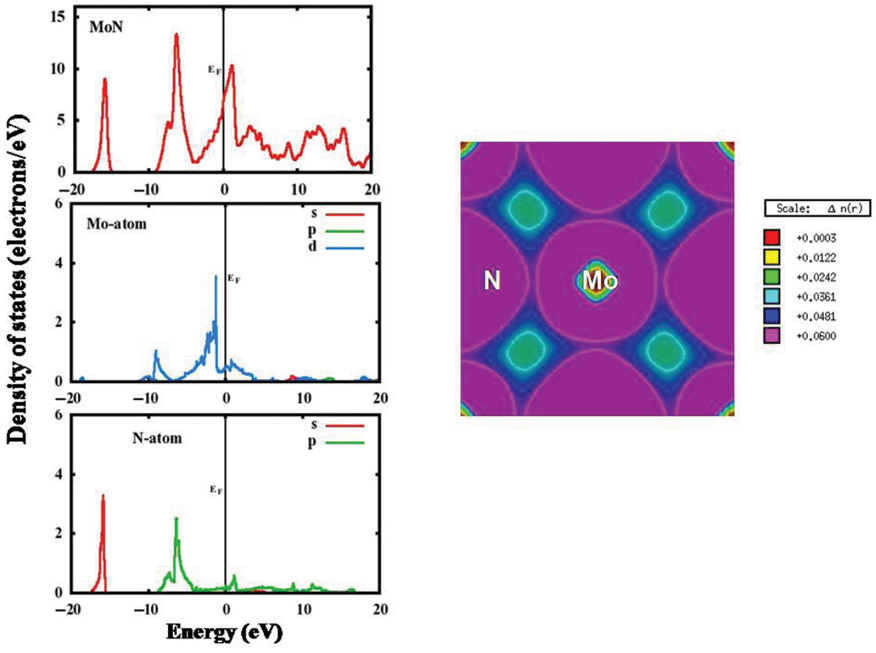

Figure 10: Electronic DOS and 2D charge density of MoN.

Cauchy pressure becomes positive for HfN and it further increases from VB to VIB groups. Therefore, the propensity of formation of metallic bonding increases from IVB to VIB groups.

The values of elastic constants also provide information about the stability of materials. The Born stability criteria for cubic crystal is given as [30]

$$C_{44} > 0, C_{11} > |2C_{12}| \text{ and } C_{11} + 2C_{12} > 0 \quad (2)$$

All TmNs follow the Born stability criteria except CrN and MoN. Both CrN and MoN exhibit $C_{11} < |2C_{12}|$ and $C_{44} < 0$, respectively. It is important to mention here that CrN exists in two forms. The CrN with orthorhombic (oP4, Pmmn) structure is stable below 285 K while the

Table 3: Calculated bulk modulus (K), elastic constants and anisotropy (A) of metal nitrides TmN (Tm = Ti, Zr, Hf, V, Nb, Ta, Cr, Mo) and available experimental data [22–25].

System	Bulk modulus (GPa)		C_{11} (GPa)		C_{12} (GPa)		C_{44} (GPa)		$A = 2C_{44}/(C_{11}-C_{12})$
	Present study	Expt.	Present study	Expt.	Present study	Expt.	Present study	Expt.	Present study
TiN	263	277, 318	508	625, 631	141	165, 171	150	163, 170	0.817
ZrN	260	240, 216	530	471	126	88	131	138	0.649
HfN	210	235, 306	453	679	89	119	84	150	0.462
VN	279	268	473		182		94		0.646
NbN	289	287, 292	586	608	140	134	62	117	0.278
TaN	339		686		166		63		0.242
CrN	281		408		217		9.54		0.0999
MoN	309		534		196		−58		−0.343

one with cubic (cF8, Fm $\bar{3}$ m) structure is stable above 285 K [3]. Therefore, the instability of CrN phase observed in terms of elastic constant in the present calculation can be attributed to nonequilibrium cubic structure. On the other hand, MoN with hexagonal (hP16, $P6_3/mmc$) structure exists in equilibrium phase diagram. Several unsuccessful attempts have been made in the past to synthesize MoN material with cubic structure due to theoretical prediction of high Tc [31–34]. It has been clearly demonstrated that the cubic phase is not stable even in high pressure but it is metastable [35]. Consequently, the instability ($C_{44} < 0$) observed in the present calculation can again be attributed to metastable cubic structure of MoN.

The values of Zener anisotropy factor (A) of the TmNs are given in Table 3. If the value of A is 1, the material is isotropic and away from 1 indicates the presence of anisotropy in elastic constants. Table 3 shows that the values of A for all the TmNs are less than 1 and it decreases from IVB to VIB groups. It also decreases within the group with increase in period. This clearly indicates that the extent of anisotropy increases from IVB to VIB groups. In addition, the extent of anisotropy also decreases within the group with increase in period. For example, TiN behaves close to isotropic material while HfN has comparatively strong anisotropy. This observation is also in agreement with results obtained by Nagao et al. [5].

The effective elastic modulus of isotropic polycrystalline materials can be evaluated from the elastic constants by following two approximations namely, the Voigt [36] and Reuss [37] assumptions that provide information about the upper and lower limit. These are

$$B = B_V = B_R = \frac{C_{11} + 2C_{12}}{3} \tag{3}$$

$$G_V = \frac{C_{11} - C_{12} + 3C_{44}}{5} \tag{4}$$

$$G_R = \frac{5(C_{11} - C_{12})C_{44}}{4C_{44} + 3(C_{11} - C_{12})} \tag{5}$$

where B is bulk modulus while G_V and G_R are shear modulus values obtained by Voigt and Reuss approximations, respectively. The average value of these two estimates mentioned above is given by Hill [38] approximation. The Voigt–Reuss–Hill (VRH) average values are given by

$$B_H = \frac{B_V + B_R}{2} \tag{6}$$

$$G_H = \frac{G_V + G_R}{2} \tag{7}$$

$$E = \frac{9BG}{3B + G} \tag{8}$$

$$\upsilon = \frac{3B - 2G}{2(3B + G)} \tag{9}$$

where B_H, G_H, E and ν are bulk modulus, shear modulus, Young's modulus and Poisson's ratio, respectively.

The calculated Bulk modulus B ($= B_H$) values of TmNs are given in Table 3. Some of the calculated values of bulk modulus are in good agreement with the available experimental data [39]. The bulk modulus values decrease within IVB group while increasing in groups VB and VIB with

increase in period. A definite trend observed from IVB to VIB groups within the same period can therefore be attributed to the addition of one valence d-electron that contributes towards strong bonding. Grossman et al. [4] have also observed similar trend and attributed this behaviour to the addition of valence d-electrons.

The calculated Shear modulus (G) and Young's modulus (E) values are given in Table 4 which do not reflect definite trend either within the group or from IVB to VIB groups. However, the calculated values in the present study for groups IVB and VB nitrides are comparatively in good agreement with those experimentally observed [39]. It is to be noted that the negative values of Shear and Young's modulus of MoN are related with instability of the phases as mentioned above. Poisson's ratio (v) values, on the other hand, reflect definite trends in both within the group as well as from IVB to VIB groups within the same period (Table 4). These values increase within the group with increase in period and also increase from IV to VIB groups within the same period. It is important to mention here that the values of Poisson's ratio are interlinked with both G and E which do not follow a definite trend as mentioned above. The experimental values of Poisson's ratios reported in the literature are in good agreement with the present calculations [39].

The values of shear and bulk modulus can also be utilized to predict the brittle and ductile behaviour of materials [40]. This can be envisaged by taking the ratio G/B. The ratio $G/B = 0.57$ is associated with brittle, otherwise related with ductile behaviour. It is clear from Table 3 that the groups IVB and V–VIB nitrides are brittle and ductile, respectively. In fact the ratio for HfN is very close to brittle to ductile transition value.

In addition, the melting temperature (T_M) of the materials can be roughly estimated using elastic constant (C_{11}) and bulk modulus [41]. The T_M for cubic structure materials can be given as

$$T_M = 553 + 5.91C_{11} \pm 300 \quad (10)$$

$$T_M = 607 + 9.3B \pm 500 \quad (11)$$

where T_M, C_{11} and B are the melting temperature, elastic constant and bulk modulus, respectively. The values of T_M for the TmNs have been estimated using the empirical equations (10) and (11) and compared with the experimental available data (Figure 11) [42]. These estimated

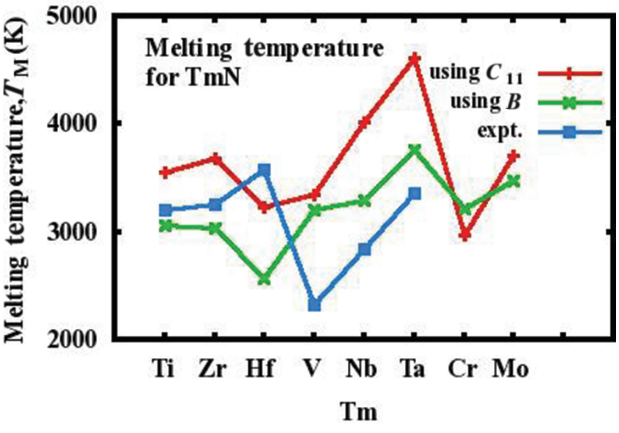

Figure 11: Estimated and experimental melting temperatures of TmNs.

Table 4: Calculated Bulk modulus (B), Shear modulus (G), Young's modulus (E) and Poisson's ratio (v) of TmNs (Tm = Ti, Zr, Hf, V, Nb, Ta, Cr, Mo) and reported experimental values [35].

System	Bulk modulus (GPa)		G_v (GPa)	G_r (GPa)	G (GPa)		E (GPa)		v	
	Present study	Expt.			Present study	Expt.	Present study	Expt.	Present study	Expt.
TiN	263	277	163.4	161.8	162.6	187	405	463	0.2439	0.220
		318				189		469		0.254
ZrN	260	216	159.4	152.4	156	138	390	390	0.2506	0.186–0.250
		240				155		392		
HfN	210	235	123.2	107.06	115	150	292	333	0.2685	0.259–0.350
		306				175				
VN	279	268	114.6	109.5	112	156	296	393	0.3229	0.256
NbN	289	287	126.4	87.2	107	117	285	387	0.3353	0.275
		292								
TaN	339		141.8	90.4	116		313		0.3464	
CrN	281		43.9	14.9	29		85		0.4494	
MoN	309		32.8	−125.3	−46		−146		0.5789	

values exhibit reasonably good agreement with calculated B than those of the C_{11} for all nitrides.

Conclusions

1. First principles DFT within GGA has been utilized to investigate the structural stability and mechanical properties of TmNs.
2. The lattice constant values of TmNs increase with increasing the atomic radii of the *T*m. Stability of the TmNs decreases from IVB to VIB groups due to increase in formation energy/atom.
3. Bonding characteristics of the TmNs have been explained based on electronic DOS and charge density.
4. All the TmNs satisfy the Born structural stability criteria in terms of elastic constants except CrN and MoN that do not exist in equilibrium binary phase diagrams.
5. The groups IVB and V–VIB nitrides are associated with brittle and ductile behaviour based on G/B ratio, respectively.

Acknowledgment: The authors are grateful to the Ministry of Defence, Government of India, for financial support. The authors are indebted to Dr. Amol A. Gokhale, Director, Defence Metallurgical Research Laboratory (DMRL), Hyderabad, for his encouragement and Dr. R. Sankarasubramanian for many fruitful discussions. They extend their thanks to Director ANURAG, Hyderabad, for the provision of computational facilities and Shri A. Mondal for technical support.

References

[1] R. Buhl, H.K. Pulker and E. Moll, Thin Solid Films, 80 (1981) 265–270.
[2] R.B. Kaner, J.J. Gilman and S.H. Tolbert, Science, 308 (2005) 1268–1269.
[3] P. Villars and L.D. Calvert, *Pearson's Handbook of Crystallographic Data for Intermetallic Phases*, ASM International, Materials Park OH (1991) 44073.
[4] J.C. Grossman, A. Mizel, M. Côté, M.L. Cohen and S.G. Louie, Phys. Rev. B, 60 (1999) 6343–6347.
[5] S. Nagao, K. Nordlund and R. Nowak, Phys. Rev. B, 73 (2006) 144113–144116.
[6] J. Chen, L.L. Boyer, H. Krakauer and M.J. Mehl, Phys. Rev. B, 37 (1988) 3295–3298.
[7] R. Nowak, F. Yoshida, Y. Miyagawa and S. Miyagawa, Nucl. Instrum. Methods, Phys. Res. B, 148 (1999) 232–237.
[8] Y. Gotoh, M.Y. Liao, H. Tsuji and J. Ishikawa, Jpn. J. Appl. Phys., 42 (2003) L778–L780.
[9] P. Hohenberg and W. Kohn, Phys Rev., 136 (1964) B864.
[10] W. Kohn and L. Sham, J. Phys. Rev., 140 (1965) A1133.
[11] Ab initio calculations, (1998–2006). http://www.abinit.org
[12] X. Gonze et al., Comput. Mater Sci., 25 (2002) 478–492.
[13] X. Gonze, Z. Kristallogr., 220 (2005) 558–562.
[14] X. Gonze et al., Comput Phys. Commun., 180 (2009) 2582–2615.
[15] J.P. Perdew, K. Burke and M. Ernzerhof, Phys. Rev. Lett., 77 (1996) 3685–3688.
[16] S. Goedecker. SIAM J. Sci. Comput., 18 (1605) 1997.
[17] M.C. Payne, Rev. Mod. Phys., 64 (1992) 1045–1098.
[18] X. Gonze, Phys. Rev. B., 54 (1996) 4383–4386.
[19] H.J. Monkhorst and J.D. Pack, Phys. Rev. B, 13 (1976) 5188–5192.
[20] A.J. Kokalj. Mol Graphics Modell., 17 (1999) 176–179. http://www.xcrysden.org.
[21] H.W. King, J. Mater. Sci., 1 (1966) 79–90.
[22] X.J. Chen, V.V. Struzhkin, Z.G. Wu et al., Proc. Natl. Acad. Sci., 102 (2005) 3198–3201.
[23] H.L. Brown, P.E. Armstrong and C.P. Kempter, J. Chem. Phys., 45 (1966) 547–549.
[24] J.O. Kim, J.D. Achenbach, P.B. Mirkarimi, M. Shinn and S.A. Barnett, J. Appl. Phys., 72 (1992) 1805–1811.
[25] V.P. Zhukov, V.A. Gubanov, O. Jepsen, N.E. Christensen and O.K. Anderson, J. Phys. Chem. Solids, 49 (1988) 841–849.
[26] B. Alling, A. Karimi and I.A. Abrikosov, Surf. Coat. Technol., 203 (2008) 883–886.
[27] K. Chen, L.R. Zhao and J.S. Tse, J. Appl. Phys., 93 (2003) 2414–2417.
[28] D.G. Pettifor, Mater. Sci. Technol., 8 (1992) 345–349.
[29] A. Riedl, R. Daniel, M. Stefenelli, T. Schöberl, O. Kolednik, C. Mitterer and J. Keckes, J. Scr. Mater., 67 (2012) 708.
[30] M. Born, Proc. Cambridge Philos. Soc., 36 (1940) 160.
[31] E.J. Saur, H.D. Schechinger and L. Rinderer, IEEE Trans. Magn., 17 (1981) 1029.
[32] N.J. Savvides, J. Appl. Phys., 62 (1987) 600–610.
[33] A. Bezinge, K. Yvon, J. Muller, W. Lengaurer and P. Ettmayer, Solid State Commun., 63 (1987) 141–145.
[34] B. Cendlewska, A. Morawski and A. Misiuk, J. Phys. F (Metal Phys.), 17 (1987) L71.
[35] L.L. Jing Chen, B.H. Krakauer and M.J. Mehl, J. Phys. Rev. B, 37 (1988) 3295–3298.
[36] W. Voigt, Lehrburch Der Kristallphysik, Teubner, Leipzig (1928).
[37] A. Reuss, Ztschr Angew. Math. Mech., 9 (1929) 49.
[38] R. Hill, Proc. Phys. Soc. London A, 65 (1952) 349–454.
[39] X.G. Lu, M. Selleby and Bo. Sundman, Acta Metall., 55 (2007) 1215–1226.
[40] S.F. Pugh, Philos. Magn., 45 (1954) 823–843.
[41] M.E. Fine, L.D. Brown and H.L. Marcus, Scripta Metall., 18 (1984) 951–956.
[42] A.W. Weimer, Carbide, Nitride and Boride Materials Synthesis and Processing, Chapman and Hall, London (1997).